WILEY

Research Article

Optimizing Niosomal Formulations for Enhanced Cellular Applications

A Comparative Case Study With L-α-Lecithin Liposomes

Nilufer Cakir [ID],[1] **Naile Ozturk** [ID],[2] **Asli Kara** [ID],[3] **Ali Zarrabi** [ID],[4,5] **and Nur Mustafaoglu** [ID][1,6]

[1]*Faculty of Engineering and Natural Sciences, Sabanci University, Tuzla, Istanbul 34596, Türkiye*
[2]*Department of Pharmaceutical Technology, Faculty of Pharmacy, Inonu University, Malatya, Türkiye*
[3]*Department of Molecular Biology and Genetics, Faculty of Arts and Sciences, Hitit University, Çorum, Türkiye*
[4]*Department of Biomedical Engineering, Faculty of Engineering and Natural Sciences, Istinye University, Istanbul 34396, Türkiye*
[5]*Department of Research Analytics, Saveetha Dental College and Hospitals, Saveetha Institute of Medical and Technical Sciences, Saveetha University, Chennai 600 077, India*
[6]*Sabanci University Nanotechnology Research and Application Center (SUNUM), Tuzla, Istanbul 34596, Türkiye*

Correspondence should be addressed to Nur Mustafaoglu; nur.mustafaoglu@sabanciuniv.edu

This study delves into the optimization of niosomal production for biological applications, focusing on their emerging role as amphiphilic nanoparticles derived from nonionic surfactants, poised at the forefront of biomedical research. We aimed to formulate and characterize a diverse array of niosomal nanoparticles, with particular emphasis on process-related parameters and physicochemical characteristics. Critical thresholds for size, polydispersity, and zeta potential were established to identify parameters crucial for optimal niosomal formulations through a comprehensive investigation of concentrations, sonication times, ingredient ratios, and surfactant types. Leveraging MODDE software, we generated 10 optimized formulations from preliminary parameter screening. The proposed experimental model design by the software exhibited acceptable similarity to the obtained experimental results (*F*-score: 0.83). The criteria for selection of the predicted experimental model formed based on targeted physicochemical considerations. To enhance half-life and penetration, especially in higher electrostatic regions like the central nervous system (CNS), we proposed a neutralized surface charge (−10 to 10 mV) while maintaining size within 100–200 nm and polydispersity below 0.5. Extended stability screening revealed periodic and extended Gaussian distributions for size and zeta potential to minimize flocculation and coagulation caused by neutralized surface charge. Notably, the cellular response performance of optimized niosomes was assessed via cellular binding, uptake, and viability in comparison with liposomes. Glioblastoma cell line (U-87) and granulocyte colony-stimulating factor (G-CSF) containing lymphoblastic leukemia cell line (NFS-60) were chosen to represent tumors developed in the CNS region and white blood cells, respectively, enabling a comprehensive comparative analysis with liposomes. The meticulous comparison between niosomes and liposomes revealed comparable cellular viability profiles on both U-87 and NFS-60 cell lines, highlighting their similarities in cellular interactions. Moreover, selected niosomal formulations demonstrated exceptional cellular uptake, either equaling or surpassing observed liposomal uptake. One of the most promising niosomes was selected and optimized to evaluate drug encapsulation performance of niosomes for further drug delivery adaptations by one of the chemotherapy drugs, paclitaxel (PTX). Cytotoxicity study was established with the most efficiently encapsulated niosomal condition with human-derived fibroblasts (HDFs) and U-87 as the representation of healthy and cancerous cell lines. Results demonstrated 1:100 diluted PTX-loaded niosome in the certain concentration demonstrated favorable toxicity in U-87 than original PTX at the same concentration while not disturbing healthy HDFs. These findings underscore the potential of niosomes for reliable drug delivery, challenging the dominance of liposomal vehicles and presenting economically viable nanocarriers with significant implications for advancing biomedical research.

1. Introduction

Niosomes are one of the promising pseudolipid nano-structures for the delivery of natural agents and drugs, which have gained acceptance as structural analogs of liposomes in the development of drug delivery strategies. Niosomes have become particularly popular for drug delivery in recent years due to their amphiphilic, biocompatible, biodegradable, and nontoxic properties. Unlike liposomes, niosomes have a vesicle construct that contains nonionic surfactants and forms a bilayer that provides better bioavailability by increasing residence time and decreasing renal clearance [1–4]. Niosomes are useful not only for drug delivery but also for targeted drug transport mechanisms such as antigens and small molecules [5]. Due to the use of nonionic surfactants, they are a cost-effective alternative; their longer chemical stability also makes them a promising candidate for drug delivery applications [1, 4, 6, 7]. They can encapsulate the drug into vesicles that improve drug bioavailability, therapeutic efficiency, and penetration through the tissue, release the drug in a sustained and controlled manner, and can be targeted to the desired site by adjusting the composition, which helps to reduce side effects [8].

Advances of niosomes are not sufficient to develop cost-effective alternatives to liposomes. The cellular application gap between niosome and liposome is needed to be filled and well-understood in the literature. Several studies have demonstrated the advantages of lipid nanoparticles as smart drug carriers through active or passive targeting [9–11]. In parallel, there are niosomal nanoparticles designed more cost-effectively and demonstrated improved encapsulation yields, resulting stable, and reproducible nanocarrier formulations [12]. However, simultaneous comparison with liposomes and exact cellular application performance were not reported to demonstrated the cost-effective alternative of liposomes. Additionally, the influence of surfactants on the physical properties of niosomal nanoparticles has been explored as enhancer toward the stability compared to lipid nanoparticles. Nevertheless, most studies have focused on drug-loaded lipid or pseudolipid nanoparticles, particularly in vitro testing and drug release profiling, while little attention has been paid to the properties and characteristics of niosomal nanoparticle formulations and cellular performance differences/similarities with liposomes that can be effectively used in drug delivery purposes.

The critical process attributes for reproducing niosomal nanoparticles and achieving appropriate cellular interactions with them are main considerations, specially from the drug delivery framework [2, 3, 13–16]. Thus, while this study may lead to effective drug delivery profiles, the potential alternatives to liposomes may literally be recorded based on their simultaneous performance. Therefore, the main objective of this study is to optimize the physicochemical and biological properties of drug-free niosomal nanoparticles, which have not been extensively studied in the literature with preliminary set criteria by the concern of crossing blood–brain barrier (BBB). Niosomes have been investigated for various drug delivery mechanisms, such as targeted and controlled drug delivery across the BBB (temozolomide) [13] and the eyes (tacrolimus, naltrexone HCl) [17] transdermally (gallidermin, clomipramine) [18], pulmonarily (glucocorticoid) [19], and orally (cefdinir, lornoxicam) [2]. Synchronous delivery of anticancer drugs via niosomes has been used for doxorubicin and curcumin [20, 21].

The design of excipients for drug development requires compliance with several commitments, including optimization of the nanostructure formulation with respect to factors such as penetration, minimum effective concentration, minimum toxic concentration, bioavailability at the site of action, frequency and route of administration, and physicochemical state [22]. Because of obligations, the carrier formulation and its optimization are as important as the drug itself [22]. To achieve the optimal drug carrier formulation, it is critical to characterize the parameters related to nanoparticle geometry [23], physicochemical properties [6, 7, 24, 25], cellular toxicity [24, 26], cellular uptake [27, 28], and species-specific abundances [29, 30]. A few studies have used formulation-dependent optimization strategies, yet niosomal formulations can be quite critical in biological applications, as demonstrated by the example of surfactant composition and surface charge of niosomes, which have a tremendous impact on the oral adsorption of repaglinide [31]. On the other hand, the influence of surfactant type and production parameters such as concentration, sonication time, temperature, and surfactant/cholesterol ratio on drug delivery has not been fully elucidated, simultaneously [3, 32, 33]. There is ample evidence in the literature that niosomes are an alternative to liposomes in terms of efficacy, safety, and stability, but the lack of reliable and reproducible niosomal formulations remains still as a limitation for transiting of these literature findings into the clinic [34–36]. Therefore, it is necessary to conduct further characterization studies of niosomal formulations to optimize the process parameters for their reliable and reproducible production.

Here, we emphasize the importance of preliminary analytical characterization of drug carriers, niosomes, and propose several niosomal formulation alternatives with critical process parameter evaluation. Overall, preliminary physicochemical characterizations, cellular toxicity, cellular uptake, drug encapsulation performance, and formulation-specific frequencies to address carrier-mediated critical parameters and simultaneous comparison with liposome nanostructures from the same analytical perspective provide evidence to the literature on the compatibility of niosomes, with the goal of more cost-effective production approach than liposomes for drug delivery, not only for research-based studies but also for the pharmaceutical industry. Figure 1 shows the general outline of the study and clarifies the perspective of the study.

2. Materials and Methods

2.1. Materials. Span 60 (Sigma-Aldrich, Germany), Tween 80 (Sigma-Aldrich, Germany), fluorescein isothiocyanate (FITC) (Sigma-Aldrich, Germany), L-α-lecithin, and cholesterol (Chol) (Sigma-Aldrich, Germany) were purchased
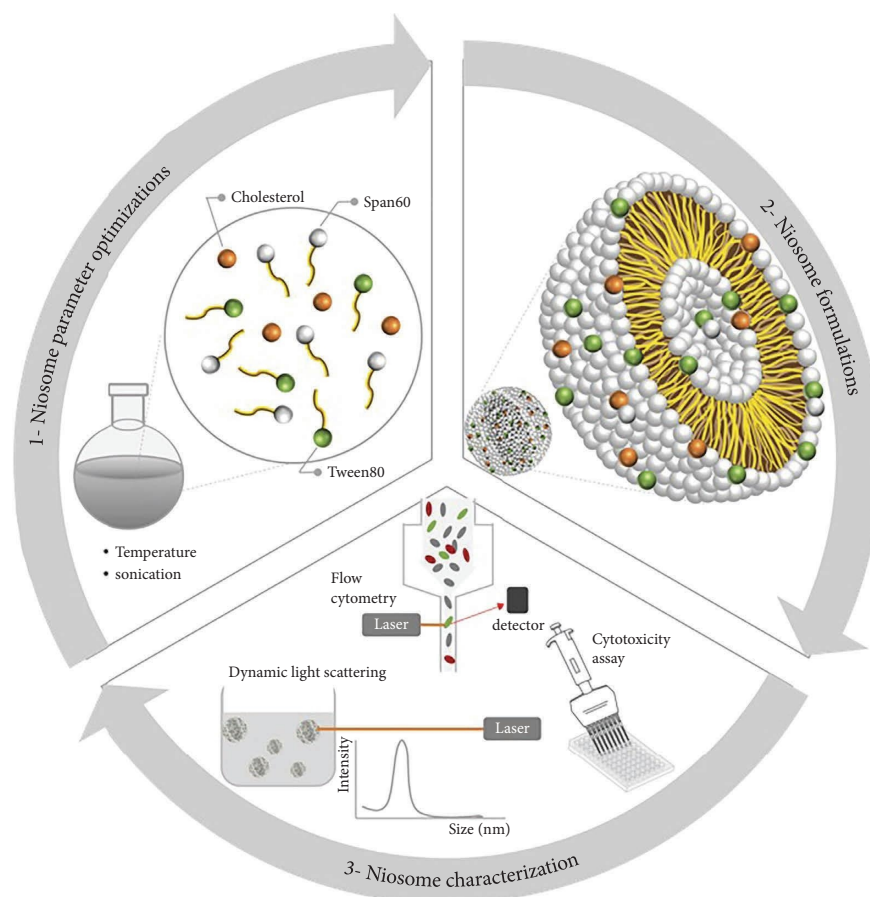
FIGURE 1: Overall study perspective for determining quality attributes and critical process parameters of niosomes used in drug delivery system.

from Sigma-Aldrich Chemical Co. Chloroform was purchased from Merck (Germany). 3-(4,5-Dimethylthiazol-2-yl)-2,5-diphenyltetrazolium bromide (MTT) was purchased from Merck (Germany). The U-87 cell line was a kind gift from Esendagli Group at Hacettepe University (Turkey). The NFS-60 cell line was a gift from ILKOGEN Biotech. All organic solvents were analytical grade, and deionized distilled water was obtained from Merck Millipore with a fixed 18.2-Ω conductivity.

2.2. Preparation of Niosomes [37]. Various niosomal formulations (Table 1) containing different types of surfactants and molar ratios were prepared using the thin-layer hydration technique [34, 38, 39]. The appropriate amount of cholesterol and surfactants was dissolved in a mixture of ethanol and chloroform (0.1:1 v/v) in a round-bottom flask with a final volume of 50 mL. The formulations are classified as multiple-surfactant type formulations (MSTF) and single-surfactant type formulations (SSTF). Three different molar ratios for MSTF and two types of surfactants for SSTF in a molar ratio of 1:1 with cholesterol were established as preliminary niosomal characterizations. A total of five different formulations were formed and designated as Formulation A, Formulation B, Formulation C, Formulation D, and Formulation E. Four different final solution concentrations were set as final

solution concentration, and composition (%) in mass was considered for ingredients by considering the final solution concentrations. Two different sonication times, 45 and 90 min, were set and applied for all five types of formulations. All preliminary experimental conditions are represented in Table 1. Each formulation was prepared in triplicate, at four different concentrations, and with two different sonication times; therefore, 24 samples were prepared for each formulation, resulting in a total of 120 samples. The organic phase was removed at 60°C under vacuum using a rotary evaporator (Heidolph, Germany). The vacuum time was set at 1 h for all formulations, and the dried thin film was hydrated with 10 mL of phosphate-buffered saline (PBS) (Sigma-Aldrich Co., Germany) at 60°C by gently shaking the round-bottom flask until all the dried film was dissolved. Each prepared formulation was treated in a sonication bath (ISOLAB, Turkey) for 45 and 90 min, respectively. In this study, sonication time is identified as a critical factor in controlling nanoparticle size, with an optimal range minimizing particle size. Insufficient or excessive sonication can lead to suboptimal outcomes, such as increased particle size or potential nanoparticle degradation. Therefore, sonication times above and below the reference value of 60 min were evaluated to determine the optimal duration for achieving the desired nanoparticle size range in nanometers.

TABLE 1: Preliminary screened formulations A, B, C, D, and E ingredient and condition list.

Formulation	Composition (%)			Formulation type	Final solution concentration (mM)	Sonication time (min)
	Span 60	Cholesterol	Tween 80			
A	25	50	25	MSTF	0.1	
B	50	50	—	SSTF	0.2	45
C	—	50	50	SSTF	0.3	90
D	30	40	30	MSTF	0.42	
E	35	50	35	MSTF		

Abbreviations: MSTF, multiple-surfactant type formulations; SSTF, single-surfactant type formulations.

2.3. Preparation of Niosomal Nanoparticles [33, 37]. The experimental process began with careful preparation, combining surfactants and cholesterol within round-bottom bottles, dissolved in chloroform to achieve a consistent liquid. Utilizing a rotary evaporator under controlled conditions at 60°C and adjusted vacuum settings resulted in the formation of a thin layer at the bottle's base. Subsequent hydration using PBS (Sigma-Aldrich, Germany) followed by ultrasonic treatment generated milky-white pseudolipid nanoparticles.

Fine-tuning parameters of niosomal production were originated via thin-film hydration method followed by sonication for achieving desired size and homogeneity. Sonicated mixtures at the determined conditions were filtered via several membrane filtering and transferred to amber glass vials for long-term preservation at 2–8°C. The pore sizes of the membrane filters were 200 μm and 100 μm, respectively. Additional filtering may be required depending on the final mixture concentration. The synthesis aimed for nanoparticles ranging from 100 to 200 nm with homogeneity between 0.2 and 0.5, employing a "thin-film layer" technique [33], explicated in Figure 2.

The methodology involved precise initial composition preparation, the use of a rotary evaporator for controlled dissolution, hydration with PBS, and sonication for nanoparticle synthesis. Subsequent optimization, filtration, and comprehensive analysis through dynamic light scattering (DLS) (Malvern, United Kingdom) facilitated a comprehensive assessment of homogeneity, size distribution, and surface charge.

2.4. Preparation of Liposomal Nanoparticles [33]. Liposomes were prepared by thin-film hydration method [38]. L-α-Lecithin (3.3 mg/mL) and cholesterol (0.8 mg/mL) were dissolved in chloroform. The lipid mixture in chloroform solution was placed in a round-bottom flask, and the chloroform was evaporated using rotary evaporator (150 rpm, 55°C, 332 mbar) to form a lipid film on the sides of the round-bottom flask. The resulting dry lipid film was hydrated with 3 mL of PBS (pH 7.4). For extrusion, the resulting lipid vesicles were passed through polycarbonate membranes of 0.6, 0.4, and 0.2 μm pore sizes, respectively, which is different from niosomal uniformity. Liposomes were then placed in a dialysis bag (3500 Da MWCO, regenerated cellulose membrane, Sigma-Aldrich, Germany) and dialyzed against PBS (pH 7.4) for 16 h. Size, polydispersity, and zeta potential measurement data for liposomes are given in Supporting Table 6.

2.5. DLS Measurements. Physicochemical characterization was obtained by DLS (Malvern Panalytical, United Kingdom) with fixed and optimized experimental procedure. Briefly, each formulation was prepared as triplicates and 13 iterations were arranged for each run. 1:10 diluted PBS at pH 7.4 was assigned as blank before each triplicate to zeroize the system. Viscosity of niosomes was set as 1.48 ± 0.01 (mPa·s) [39]. To measure the size and homogeneity of formulations, polystyrene cuvettes (Malvern Panalytical, United Kingdom) were used. To measure zeta potential of each formulation, capillary zeta cell cuvettes (Malvern Panalytical, United Kingdom) were used.

2.6. Fluorescence Labeling of Niosomes. Niosomes were labeled with FITC (Sigma-Aldrich, Germany) dissolved in ethanol at the fixed concentration and incubated overnight after rotary evaporation following the previously published thin-film hydration protocol [40, 41]. Each niosomal formulation is tagged by 300 nM FITC stock solution with two different mixing ratios (1:50 and 1:100 v/v). FITC was entrapped inside of niosomes, and excessive FITC was removed by continuous sterile filtering. Encapsulation efficiency (EE) (%) of FITC was calculated based on the former FITC-load absorbance and released FITC absorbance after centrifugal removal by using the equation demonstrated as equation (1). The FITC concentration was calculated based on FITC-based standard curve demonstrated in Supporting Figure 6. Each labeled formulation was physiochemically characterized after the labeling procedure by DLS with a dilution factor of 1:10 in PBS to determine whether its behavior changed in terms of size, charge, and polydispersity. The tagging of niosome-FITC was only generated for cellular uptake purposes. Calculated EE% for tagged niosomal formulations is demonstrated in Supporting Figure 11:

$$EE\,(\%) = \frac{\text{total amount of released FITC}}{\text{Initial Load of FITC}} x100. \quad (1)$$

2.7. Fluorescence Labeling of Liposomes. The liposomes were labeled with FITC using freeze–thaw cycles [19, 42, 43]. The method of freeze–thaw was accomplished after formation of liposomes. Thus, freeze–thaw cycles with the same amount of FITC were utilized to liposome followed by using extruder with 200-μm polycarbonate filtering. This involved
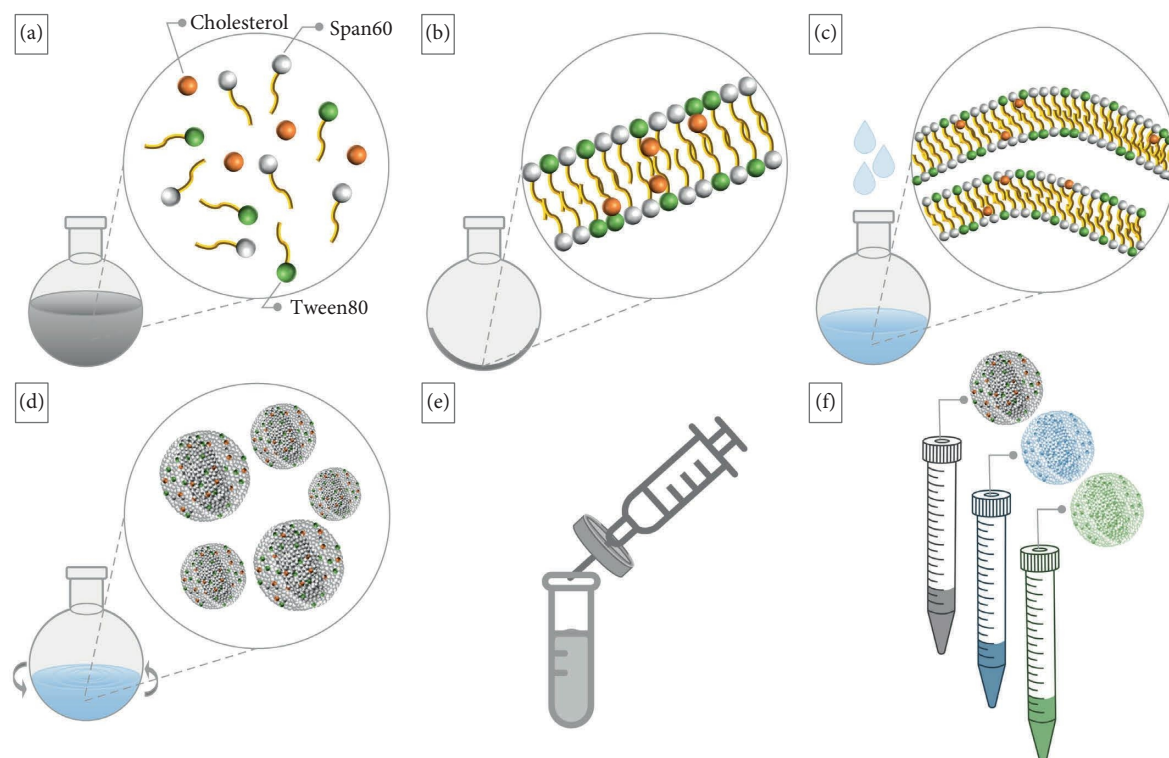
FIGURE 2: Thin-film layer method for preparation of niosomes. (a) Surfactant and cholesterol mixture. (b) Evaporation of organic solvent. (c) Hydration. (d) Hydration with sonication. (e) Sterile filtration under the fume hood for further characterizations. (f) The collection of final niosomal nanoparticles.

subjecting the labeled liposomes to six subsequent freezing and thawing cycles, each cycle occurring every 4 h. These cycles may induce stress on the liposomal membrane due to ice crystal formation during freezing [42]. Therefore, FITC-tagged liposomes were checked via DLS after extruding and before treating with the cells to verify the preset required physicochemical specifications. Any excess FITC after freeze–thaw cycles were eliminated through 0.2-μm membrane filtration. Subsequent tracking of the size and homogeneity of the tagged liposomes allowed for simultaneous comparison with tagged niosomal nanoparticles, revealing expected levels of size, PDI, and zeta potential. Additional details can be found in Supporting Table 6.

2.8. Drug Loading of Niosomes. Paclitaxel (PTX) (ATAXIL, DEVA Pharmaceuticals) was encapsulated by niosomes to determine their potential drug loading capacity (DLC%) and drug loading efficiency (DLE%) for future studies. PTX-loaded niosomes were then exposed to healthy (human-derived fibroblasts (HDFs) and cancerous cell lines (U-87) to investigate their potential cytotoxicity profiles. By this purpose, one of the most promising niosomes, Opt-10, was selected for exposure. Three different loading concentrations were prepared to load the niosome, and the highest EE% corresponded concentration was selected for the toxicity studies. Required calculations are represented in equations (2)–(4). PTX standard curve was established with six different concentrations to determine EE% indicated in equation (1) and DLE% demonstrated in equation (4). All nanodrop measurements were performed at 230 nm which was established wavelength to determine PTX [44]. All drug-loaded niosomes were analyzed by DLS before toxicity assay and results demonstrated in Supporting Figures 12a and 12b:

$$\mathrm{DLC}_{\mathrm{Theoretical}}\,(\%) = \frac{\text{weight of drug in nanoparticles}}{\text{weight of nanoparticles}}\, x100, \tag{2}$$

$$\mathrm{DLC}_{\mathrm{Actual}}\,(\%) = \frac{\text{weight of entrapped drug}}{\text{weight of recovered nanoparticles}}\, x100, \tag{3}$$

$$\mathrm{DLE}\,(\%) = \frac{\mathrm{DLC}_{\mathrm{Actual}}}{\mathrm{DLC}_{\mathrm{Theoretical}}}. \tag{4}$$

2.9. FTIR Analysis. FTIR analysis was performed to verify the presence of FITC in the niosomal nanoparticles and to ensure the labeling procedure. The samples were dried by freeze-drying in glass containers. The control groups consisted of FITC only and nanoparticles only to compare whether the labeling was successful. The dried samples were analyzed by FTIR (ThermoFisher, USA) and analyzed using OMNIC software. The statistical evaluations and the raw version of the data analyzed with the software are given in Supporting Figure 8.

2.10. MODDE Analysis. Preliminary formulation screening for the investigation of final concentration, sonication time, surfactant type, and surfactant composition was evaluated by MODDE software. Design model was set based on target size range as 100–200 nm. Modeling was determined as multifactorial analysis, and significance was set as alpha: 0.5. Contour mapping mode and screening module were selected to obtain optimized formulations, and 10 different optimization formulations were obtained. Table 2 indicates MODDE Software output evaluated in logarithmic threshold.

2.11. Cell Maintenance. Glioblastoma cell line U-87 and lymphoblast cell line NFS-60 were grown as adherent and suspension cells in Dulbecco's modified Eagle medium (DMEM) (Pan Biotech, Germany) containing 10% FBS + 1% Penicillin/Streptavidin and RPMI 1640 (Pan Biotech, Germany) + 10% M-CSF (Gibco), respectively. Cells were cultured in T75 culture flasks (ISOLAB Co., Germany) at the same period (3-day culture interval) with a division ratio of 1:5.

2.12. Cell Viability Assay. All cell viability assays were performed in 96-well plates (ISOLAB Co.) by seeding 5000 cells/well in 100 μL to each well with 2-h incubation at 37°C. Except PTX-loaded niosomes and their toxicity profile, all toxicity studies with nonload niosomes were performed with 9 serial dilutions with 1:10 dilution from 1000 pM. to 10^{-5} pM. All dilutions' first stock was prepared in starvation media with 1:2 volume ratio. Niosomal nanoparticles were incubated with the cells 24, 48, or 72 h. Then, 3-(4,5-di-methylthiazol-2-yl)-2,5-diphenyltetrazolium bromide (MTT) was dissolved in PBS at pH 7.4 with a final concentration of 0.5 mg/mL, applied 50 μL on each well of the plated, and incubated 3 h. Reading of the wells was performed by removing media and adding 200 μL of solubilization solution containing 10% SDS in DMF at pH 4.6. The results of cell viability assays were obtained using a microplate reader and detected at the wavelength of 570 nm (Bio-Rad, USA).

In PTX-loaded niosomes, the highest EE% was selected and diluted as volumetric ratio within the wells. Testing groups were combined of control samples as nonloaded niosomes and only PTX. Testing samples were prepared at the concentration of 0.0125 mg/mL (the most promising PTX load, see Supporting Figure 12) PTX loaded into

niosomes (0.2 mM) and diluted to 1:100. All niosomal dilutions were prepared in the starvation media after 1-day cellular attachment. The number of cells seeded through the wells was 5000 cells/well in 100 μL with overnight incubation at 37°C. Four serial dilutions from one stock PTX-loaded niosomes (0.2 mM) were exposed to HDF and U87 cell lines for 48 h. Then, 3-(4,5-dimethylthiazol-2-yl)-2,5-diphenyltetrazolium bromide (MTT) was dissolved in PBS at pH 7.4 with a final concentration of 0.5 mg/mL, applied 50 μL on each well of the plated, and incubated 4 h. Reading of the wells was performed by removing media and adding 180 μL DMSO (Merck, Germany). The results of cell viability assays were obtained using a microplate reader and detected at the wavelength of 570 nm (Bio-Rad, USA).

2.13. Flow Cytometry Assay. U-87, GBM cell lines were seeded in 24-well plates (ISOLAB Co.) at a seeding rate of 2×10^4 cells/well. Seeded cells are adapted overnight before the assay. FITC-tagged niosomes were diluted 1:5000 and added as 1:100 ratio of total volume of the well. Passive incubation was followed by the intervals of 2, 4, 6, 8, and 10 h and collected separately with their duplicates. Trypsin (Pan Biotech) was used to remove the cells for replacing medium by centrifuge at 2000 rpm, 5 min with PBS, and repeating this step continuously three times. Final solution of cell uptake niosomes is dissolved in PBS containing 1% PFA. After optimization, total cellular uptake was performed after 6 h of incubation. Cell uptake analysis of each formulation was tested using FACS (BD, USA) with FITC-tagged niosomes. All cell uptake analyses, including the control group, were analyzed using FlowJo software and structured by layout mode with histogram-based gating.

2.14. Statistical Analysis. Prism (License number: GPWF-045319-RIE-6746 to Sabanci University, Version 5.01) was utilized for experimental statistical evaluations. One-way, two-way, and three-way ANOVAs with one-sample t-test confirmations were used for data analysis. Cell viability assay was analyzed by Graph Prism log-response sigmoidal analysis mode.

3. Results and Discussion

3.1. Optimization of Niosomal Nanoparticle Formulations and Initial Physicochemical Characterizations. Although many studies have focused on optimizing the process for drug-loaded niosomal formulations in terms of EE% and release assays [3, 45–47], a few studies have been conducted to understand the physicochemical properties of niosomes with or without drug load [12, 16]. We started with a screening of the production parameters of niosomes and their mutual synergistic effects. We used the thin-layer film hydration method for niosomal production, with each step contributing to the variables and constants of physicochemical characterization. These process parameters included surfactant type, constituent molar ratios, number of surfactants, final suspension concentration (mM), sonication time (min), transition temperature (°C), rotation speed

TABLE 2: Two-factorial effect matrix of determined niosomal production process parameters.

X	Cholesterol (%)	Span 60 (%)	Tween 80 (%)	Mixture concentration (mM)	Sonication time (min)
Cholesterol (%)	—	*	***	NS	NS
Span 60 (%)	*	—	****	NS	NS
Tween 80 (%)	***	****	—	NS	NS
Mixture concentration (mM)	NS	NS	NS	—	NS
Sonication time (min)	NS	NS	NS	NS	—

Note: NS: p value > 0.05.
* p value ≤ 0.05.
** p value ≤ 0.01.
*** p value ≤ 0.001.
**** p value ≤ 0.0001.

(rpm), organic solvent type, final suspension volume (mL), hydration buffer, and hydration volume (mL). However, the effects of many of these process parameters on the physicochemical properties of niosomes, such as size, polydispersity, and zeta potential, were unknown or had not been published before.

To perform an initial screening of the process parameters, we conducted an experiment with niosomal production parameters as listed in Table 1. We divided the formulations into SSTF and MSTF, each with four different concentrations (mM) and two different sonication times (min). The temperature was 60°C, the rotation speed for the hydration step was 150 rpm, the organic solvent was chloroform, hydration buffer was PBS, and the hydration volume was 10 mL throughout the study. Our main objective was to understand the effects of concentration (mM), sonication time (min), and surfactant types (MSTF vs. SSTF) on the physicochemical properties of niosomes such as size (nm), PDI, and zeta potential (mV). Figure 3 shows the overall size (nm) distribution as a function of all process variables across SSTF and MSTF of niosomes, while Supporting Figure 3 indicates size distribution across five different formulations at two different sonication times (45 min vs. 90 min). Supporting Figure 1 shows the polydispersity and zeta potential (mV) distribution profiles at different concentrations (0.1, 0.2, 0.3, and 0.42 mM) for all formulations. To consider concentration variable (controlled) to size variable (uncontrolled), two-way ANOVA statistical consideration is applied. By that, the effect of concentration on size was aimed to be determined. To consider the separate investigation for sonication time on the concentration variable, while sonication time was already having two different set points, unpaired t-test was applied. The effect of sonication time on the size of five different formulations is shown in Supporting Table 1. Supporting Tables 3A and 3B provide further details on two-way ANOVA for the PDI and zeta potential of the preliminary formulation screening of niosomes, in addition to sonication time versus size consideration.

The correlation matrix shown in Table 2 combines two-way ANOVA and multiple *t*-tests (Supporting Table 2). The optimal process conditions for niosomal production were determined by screening three parameters: (1) ingredient percentage (%) and type of surfactant; (2) final mixture concentration and surfactant type; and (3) sonication time

(min). This preliminary screening of niosomal production parameters in Figure 3 guided to determine promising formulation recipes can be statistically optimized via MODDE. By that, factor-effect analysis was performed. Two-factorial analysis indicated in Table 2 was formed based on preliminary effect findings in Figure 3 and on required preset physicochemical specifications. In this evaluation, size, homogeneity, and zeta potential were model responses of determined process parameters. According to the preliminary determination, the most significant effect on physicochemical targets of niosomal formulations appeared when multiple surfactants were used. Such observation can be observed between Span 60 and Tween 80 correlation (**** p value ≤ 0.0001). In addition, Tween 80 has more impact on physicochemical properties than Span 60 correlated with cholesterol, *** p value ≤ 0.001 and * p value ≤ 0.05, respectively. Although there is no specific effect determined for sonication time or mixture concentration on overall responses, formulation-specific investigation may vary according to the obtained results. However, preliminary parameter screening was designed for initial effect evaluation, and thus, formulation-specific impacts were not reported. Besides, formulations from A to E were not included to further studies and only used for obtaining statically proposed formulations by MODDE.

The data obtained were statistically analyzed, and further formulations were determined using the DoE program MODDE. The optimized conditions were evaluated in a logarithmic order with the evaluation of the target size between 100 and 200 nm to ensure the nanoparticles entry into cellular and biological barriers [48, 49]. PDI and zeta potential (mV) were eliminated for the targeting step. MODDE proposed 10 different optimized experimental conditions prepared based on preliminary findings demonstrated in Figure 3. The obtained results of 10 optimized formulations were predicted by MODDE software based on previously reported data. Predicted and utilized conditions of MODDE (experimental) are listed in Table 3. By applying the proposed conditions by MODDE, we obtained niosomal nanoparticles, and their size distributions (nm) represented in a single column in Table 3 and their detailed size (nm), PDI, and zeta potential are shown in Figure 4. According to the obtained average size (nm), the overall size range of 10 optimized formulations was between 120 and 180 nm,
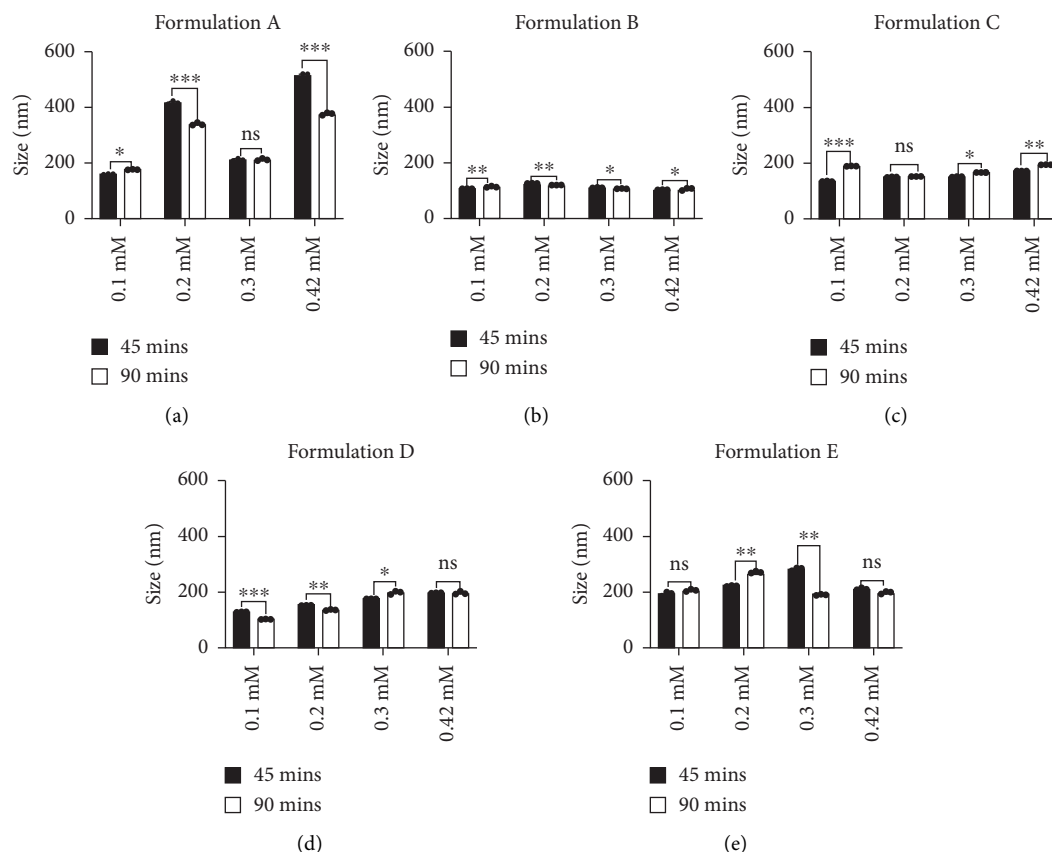
FIGURE 3: Preliminary effect analysis of sonication, final mixture concentration, and surfactant type profiled for all formulations (a–e), demonstrated in Table 1. Two-way ANOVA is applied to all preliminary formulations to identify concentration (mM) and sonication time (min) on size (nm). ns: p value > 0.05; *p value ≤ 0.05; **p value ≤ 0.01; ***p value ≤ 0.001; ****p value ≤ 0.0001. ANOVA, analysis of variance.

TABLE 3: DoE optimized formulation, ingredient, and condition list.

Molar ratio (%) (CHO:S60:T80)	Predicted size (nm)	Predicted mixture concentration (mM)	Predicted sonication time (min)	Obtained size (nm)
34.5:43.5:22	100.6	0.228	63	127.7 ± 7.11
41:2:57	99	0.126	47	125.4 ± 2.13
40:3:57	92.5	0.1	45	114.7 ± 14.14
49:49:2	97	0.125	86	142.9 ± 11.32
49:49:2	92	0.1	83	149.3 ± 12.11
48:4:48	99.8	0.11	50	110.3 ± 9.22
49:48:3	99.5	0.13	89	176.7 ± 11.12
50:50:0	84.4	0.1	90	141.3 ± 15.48
50:50:0	92	0.1	45	137.3 ± 9.23
50:50:0	97	0.2	90	145.6 ± 5.34

the PDI range was between 0.1 and 0.3, and zeta potential (mV) range was between −0.5 and 0.5 mV. The F-score similarity test was determined as 0.83. Although targeted neutralized surface charge was achieved, stability tracking was required due to their close tendency to be aggregated in such surface properties.

3.2. Testing the Stability of Niosomal Nanoparticles. Ten different optimized niosomal formulations were characterized and found to be in the critical range of size (nm),

PDI, and zeta potential (mV). Niosomes are considered to be more stable drug carriers than liposomes, but accurate stability profiles of niosomes have not been established beyond 4 weeks [12]. On the other hand, although size (nm) was followed up to 4 weeks, their PDI and zeta potential (mV) fluctuations by time were not reported. Therefore, a 92-day stability test was performed while storing the samples at +4°C. Each formulation and the variations in its size (nm), PDI, and zeta potential (mV) were compared by applying one-way ANOVA. Figure 5 shows the change in size (nm) in 92 days for each
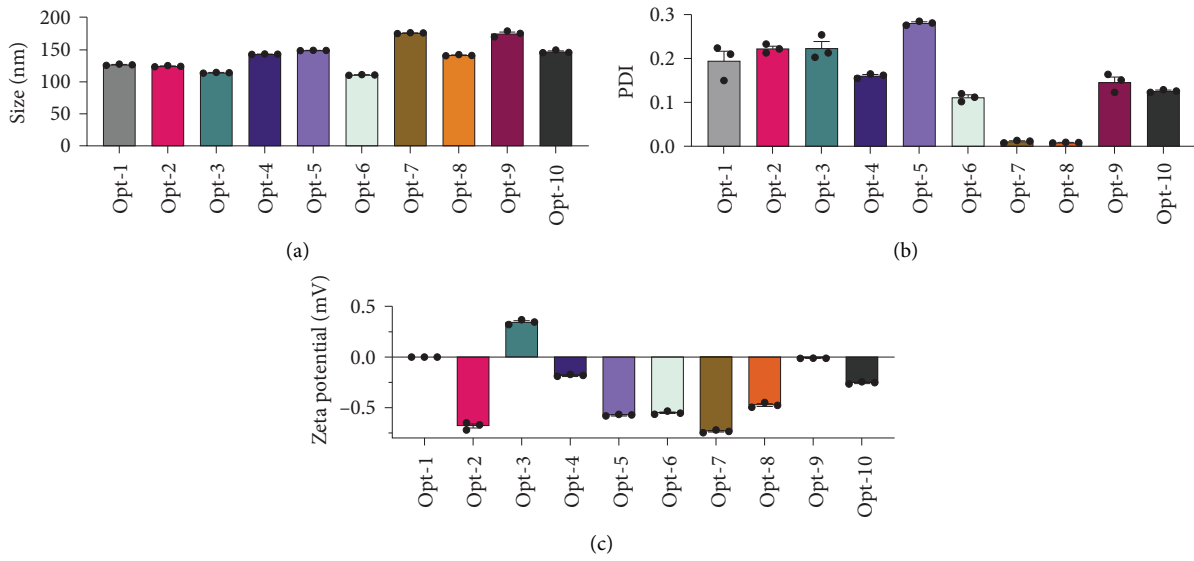
FIGURE 4: Ten different optimized niosomal formulation physicochemical profiles. (a) Size distribution (nm) (ranging from 100 to 200 nm). (b) Polydispersity (PDI) (ranging from 0.05 to 0.3). (c) Zeta potential (mV) (ranging from −0.5 to 0.5 mV). The size distribution of the data is demonstrated in Supporting Figure 9.
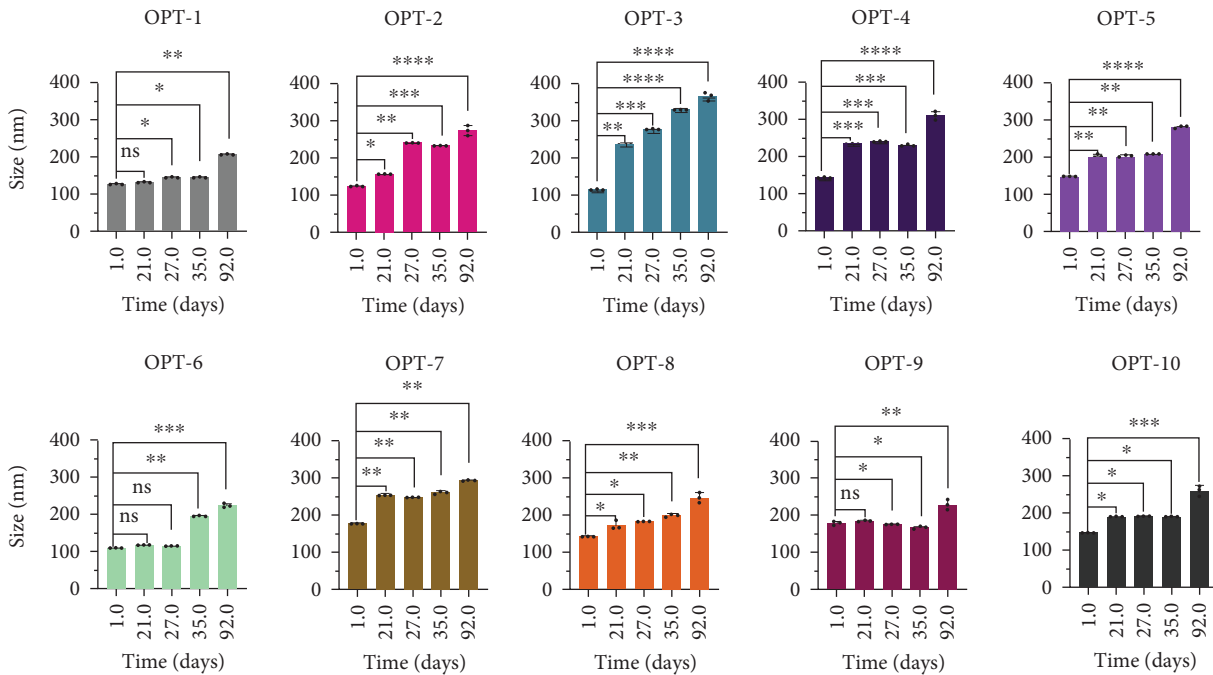

FIGURE 5: 92-day shelf-life profiling of optimized 10 formulations. One-way ANOVA is applied to all niosomal formulations to determine overall 92-day shifting profile for A. Polydispersity (PDI), B. Zeta Potential (mV). One-sample t-test is applied to each formulation and analyzed for the shift between 1 and 21 days, 1–27 days, 1–35 days, and 1–92 days in Supporting Tables 4A and 4B (ns: p value > 0.05; * p value ≤ 0.05; ** p value ≤ 0.01; *** p value ≤ 0.001; **** p value ≤ 0.0001). ANOVA, analysis of variance.

formulation. Formulations were named according to Table 3 as the order of columns from Opt-1 to Opt-10. Supporting Figure 2 demonstrates PDI and zeta potential (mV) profiles in 92 days for each optimization. The most stable niosomal formulations in terms of size (nm) were defined based on slight changes and no aggregation profiles in their peak iterations. The most stable PDI and zeta potential (mV) profiles of niosomal formulations

were determined based on sudden jumps in PDI and zeta potential (mV). Slight changes were also acceptable decision criteria for PDI and zeta potential (mV).

Supporting Tables 4A and 4B demonstrated the detailed statistical significance evaluation in their stability profiles for PDI and zeta potential (mV). In the size stability profiles, Opt-1, Opt-6, Opt-8, Opt-9, and Opt-10 showed slight changes in 92 days and were also in the critical size

range, which was set at 100–200 (nm). The PDI stability profiles demonstrated that Opt-4, Opt-5, Opt-9, and Opt-10 had slight changes in 92 days. Except for Opt-1, Opt-2, and Opt-3, the PDI of all optimized niosomal formulations was in the critical range of 0.2–0.5. The zeta potential (mV) stability profiles were in the critical range of −10 to 10 mV for all niosomal formulations. The most stable zeta potential (mV) profiles were selected as Opt-5, Opt-6, Opt-9, and Opt-10 since no fluctuations were observed in their zeta potential measurements within 92 days. Interestingly, Opt-9 was found to have a gradual increase in electronegativity over 92 days among all other optimization formulations, which was still in the range of −10 to 10 mV. Stability tests showed that five niosomal formulations were in the critical size range (nm), almost seven niosomal formulations were in the critical PDI range, and all niosomal formulations were in the critical zeta potential (mV) range in 92 days.

3.3. Testing the Reproducibility of Niosomal Nanoparticles.
To determine the reproducibility of the niosomal formulations, three experiments were performed at three different days under the same conditions as in Table 3. Comparison was made using F-score (Sorensen–Dice coefficient). The F-score test indicates the similarity of each run with respect to the different intervals between days and gave a value of 0.62. The most reproducible data among 10 formulations were obtained with Opt-10, one of the most stable optimized conditions in the size range from 100 to 200 nm. The reproducibility test was necessary to use these nanocarrier formulations in drug delivery with greater accuracy. Additionally, the reproducibility test, followed by a 92-day stability test, brought the novel results to the literature where no record of them was found before. Figure 6 demonstrated the reproducibility profile for the size (nm), and Supporting Figure 3 demonstrated the reproducibility profile for the PDI and zeta potential (mV). Based on the reproducibility profiles for the size (nm) of 10 niosomal formulations, all formulations except Opt-4, Opt-5, and Opt-7 were found reproducible. Although significant variations were observed in some formulations, they were accepted if the results were found nonexcessive within the critical ranges. Detail statistical evaluations can be found in Supporting Table 5.

3.4. FTIR Profiling for Lyophilized Niosomes and Liposomes.
FTIR analyses were performed to select certain optimized and promising niosomal formulations based on corresponded sole ingredient spectra. In Supporting Figure 8, niosomal nanoparticles and liposomes have common chemical groups with several differences. First, all niosomal formulations have demonstrated the similar wavelength ranges from 3600 to 3200 cm^{-1} which represents parallel findings to Span 60 sole spectra demonstrating O-H stretching [50]. Another spectral observation is made in the wavelength range of 2400–2600 cm^{-1} and typically corresponds to the region associated with aliphatic C-H stretching [51]. This range often includes vibrations from methyl (CH$_3$) and methylene (CH$_2$)

groups present in organic molecules. The peaks in this range can indicate the presence and nature of these aliphatic hydrocarbon chains.

L-α-Lecithin should give several wavelengths observed in 2800–3000 cm^{-1}, which corresponds to C-H stretching vibrations in the hydrocarbon chains. Another wavelength observation demonstrates the ester carbonyl stretch of the phospholipid head group within the wavelength of 1740–1750 cm^{-1}. Other phosphate group-related vibrations are observed within the wavelength of 1200–1300 cm^{-1}. Although niosome and liposome chemical groups indicate the expected wavelength ranges, determined O-H stretching and C-H stretching characteristics are changed by the formulation conditions. For instance, Opt-5 demonstrates the least concentrated O-H stretching compared to other formulations. Besides, in this region, it is clearly seen that O-H stretching is the most affected chemical group by the formulation conditions. This observation suggested the importance of process conditions applied during the synthesis, such as temperature, pressure, or duration of reactions, can affect the structure and arrangement of molecules on the nanoparticle surface, potentially impacting O-H stretching vibrations [2]. On the other hand, Opt-5 is found one of the most affected formulations from shelf-life that refers the more stable and concentrated O-H stretching promotes the stability of niosomal nanoparticles. The O-H stretching vibrations are often associated with surface-bound hydroxyl groups [51]. A decrease in O-H stretching intensity might imply fewer available hydroxyl groups on the surface, which could indicate modifications or changes in the surface chemistry. This alteration might impact the stability of nanoparticles, especially if these hydroxyl groups are involved in stabilizing the nanoparticle dispersion or in interactions with surrounding molecules. While changes in O-H stretching intensity in the FTIR spectrum can provide indications about the stability of nanoparticles, it is essential to consider multiple factors and conduct complementary analyses to draw comprehensive conclusions about nanoparticle stability and behavior. Thus, such complimentary analysis done through the study provides a deep understanding and robust formulation selection for further therapeutic functionalization.

3.5. Assessing the Cellular Toxicity of Niosomal Nanoparticles.
Physicochemical characterization of niosomal formulations, stability profiles, and reproducibility tests was performed, and promising formulations were recorded. To test their cellular toxicity, MTT assay was performed two different cell sources: U-87 and NFS-60. Supporting Figure 4 shows the cellular viability profiles of 10 different niosomal formulations and liposomes of the glioblastoma cancer cell line U-87. We screened the cellular viability profiles of these niosomal formulations after 48 days of their synthesis to determine whether the range of cellular viability had gradually shifted, as shown in Figure 6 for U-87. In addition, the leukemia cell line, NFS-60, was tested with the same niosomal formulations and liposomes (see
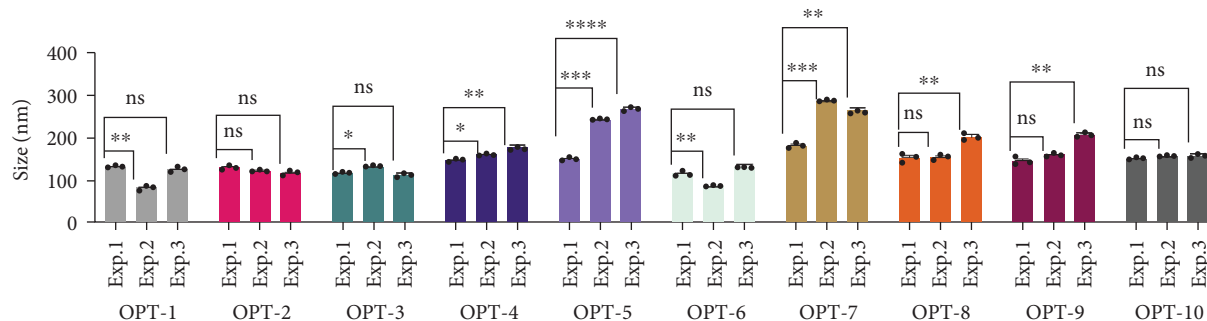
FIGURE 6: Intraday experiments of 10 optimized formulations demonstrating reproducibility performance of each in size (nm). PDI and zeta potential profiles are demonstrated in Supporting Figure 3. Unpaired t-test ANOVA statistical analysis is performed to compare and determine three interday experiment groups in the same experiment conditions. ns: p value > 0.05; * p value ≤ 0.05; ** p value ≤ 0.01; *** p value ≤ 0.001; **** p value ≤ 0.0001. PDI, polydispersity index.

Supporting Figure 5). Both of these different cell lines with the same niosomal and liposomal formulations showed no cellular toxicity and had similar cellular viability profiles. Cellular viability ranged from 80% to 100% with all 10 different niosomal formulations and liposomes when they tested only a day after their synthesis. On day 24 and day 48 after their synthesis, cellular viability ranged from 75% to 100%. The results also confirmed the stability test of the niosomal formulations, in almost all niosomal formulations were stable for at least 2 months. In order to make final decisions for further selection of optimal niosomal formulations, their cellular uptake profiles needed to be investigated.

3.6. Cellular Internalization of Niosomes. Fluorescently labeled niosomes were generated for cellular assessments. A total of 10 distinct niosomal formulations, along with liposomes labeled using the fluorescent tracer FITC, were subjected to analysis through flow cytometry [52].

FITC labeling of niosomes was based on the total volume of niosomal formulations before the production process. The overall, based on the desired last concentration, FITC existence was set to 0.05% of the total volume from the stock solution of 300 nM. The percentage of FITC and stock solution concentration are set, and EE% was calculated based on sole standard curve of FITC. Standard curve of FITC and the linear curve equation are presented in Supporting Figure 6. After encapsulation of FITC, high-speed centrifugal release (12,000 rpm, 20 min) was used, and supernatant absorbance was recorded triple to calculate the entrapment efficiency. Supporting Figure 7 indicates the stability of FITC labeling efficiency between replicates. All EE% results obtained from different FITC concentrations are demonstrated in Supporting Table 7. Results demonstrated almost all optimized niosomal formulations are gradually decreased their EE% by increased FITC concentration and not all niosomal formulation demonstrated the same EE% at the same FITC concentration. L-α-Lecithin liposomes' FITC tagging is performed after determining the optimum FITC concentration for niosomal formulations.

To utilize the formulated niosomes as improved carrier agents, investigation of their cellular uptake was critical. The cellular source U-87 was used for the study. Incubation time optimization was performed based on one of the most reliable physicochemical standings, Opt-10, and the change in FITC-A mean was analyzed by using statistical interface embedded in FlowJo. Figure 7 demonstrates the only cell population and corresponded FITC-A mean which could be also considered as baseline point for the overall FITC-A mean intensity. Flow cytometer allows three different runs from the same sample; however, intraday uptake profiles cannot be considered as one of the replicates for the same experiment. However, their trend could be comparable. Results demonstrated that after 6-h incubation, slight decrease in FITC-A mean is observed. Thus, all further cellular uptake profiling of niosomal and liposomal nanocarriers was tested in 6-h incubation.

The incubation time optimization demonstrated that long incubation period could diminish the uptake that could be caused by decreased intensity of FITC since 48-h cellular viability indicated no toxicity observed for all niosomal formulations for U-87MG and NFS-60 cell lines. After determination of the most proper incubation time, simultaneous cellular uptake profiling for niosomal and liposomal formulations was tested for 6 hours. Figure 8 demonstrates individual FITC-A mean captured for all testing groups.

The analysis conditions were set based on the sole population FITC-A mean intensity which was asset for the starting gate. The sole population was supposed to not have FITC-A count. However, FITC autofluorescence positive feed is already reported in the literature [7, 53, 54]. Thus, the recorded FITC-A intensity in sole cell population was considered as autofluorescence of FITC labeled laser taken as baseline. In the evaluation, not only forward scattered light could be enough for picking the proper formulation. The results demonstrated that x-axis or forward scattered light determined uptake is not indicating any advance or difference, means that cells remain healthy during the uptake. If so, they are not demonstrating any difference between each other. On the other hand, site-scattered light versus FITC-A mean indicates that glioblastoma cells are able to uptake the
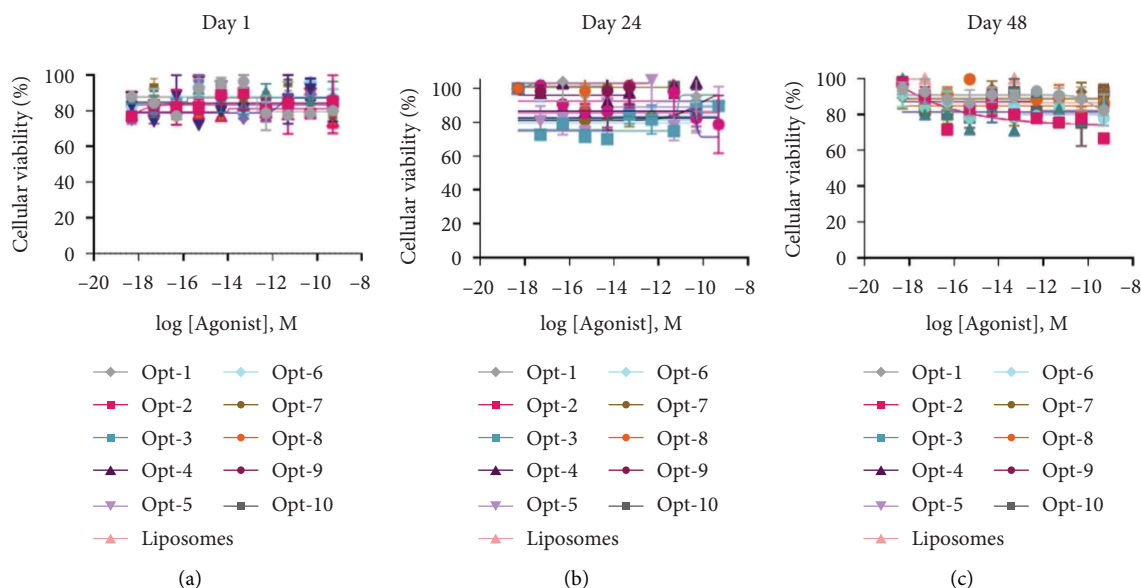
FIGURE 7: 48-day cellular viability MTT assay for all niosomal optimizations and liposomal comparison performed in U-87 cell line. (a) Day 1 cell viability (%) in the range of 80–100. (b) Day 24 cell viability (%) slow shift to the range of 75–100. (c) Day 48 cell viability (%) slow shift to the range of 75–100. 5000 cells/wells are used, and 9 serial dilutions are applied. Sigmoidal log-response concentration (M) indicates the x-axis.
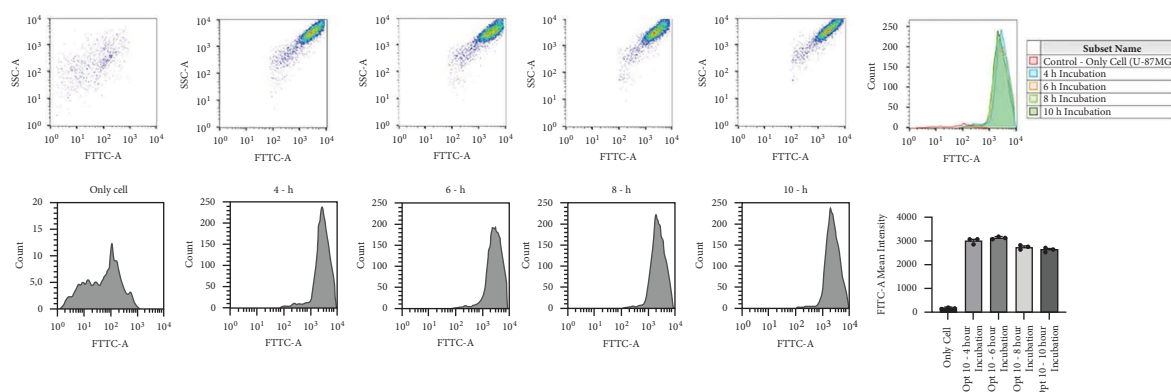

FIGURE 8: Different incubation time screening profiles for cellular uptake in 4, 6, 8, and 10 h. FITC-A mean distribution which is normalized based on internal loading control is graphed and selected based on the highest FITC-A mean. Each formulation cellular uptake is obtained as triplicate from the same population, different well plates. 2×10^4 U-87 cells are used for each FITC-tagged niosomes. FITC, fluorescein isothiocyanate.

niosomal nanoparticles in the y-axis manner. It means the uptake should be analyzed in both ways as it is demonstrated in Figure 9.

Cellular internalization analysis initiated with seeking for optimum internalization time sets that were not previously reported. To utilize the same internalization time, several simultaneous analytical considerations were made. Initially, same FITC amount was utilized to all nanocarriers to not cause any false-positive signal results. The similar consideration is accomplished in seeded cell number equality. Since seeded concentration and incubation time in their internalization were also same, the only variance was nanocarrier formulations itself. In Figure 9, x-axis evaluation was normalized and subtracted from the only

cell FITC-A signal. However, x-axis change indicates overall granulation inside the cell after uptake of nanocarrier. Thus, the change in x-axis becomes normal and indicates that all tested niosomal and liposomal nanocarriers were having similar uptake performances that made the decision even harder. On the other hand, there were significant signal differences observed in y-axis and thought to be alternative path to evaluate nanocarrier performance difference between niosomal and liposomal nanocarriers. Evaluation in y-axis could give the idea of attachment for nanocarriers on the surface of cells and could become longer in length of cells. Therefore, y-axis evaluation was normalized and graphed by subtracting only cell FITC-A signal.
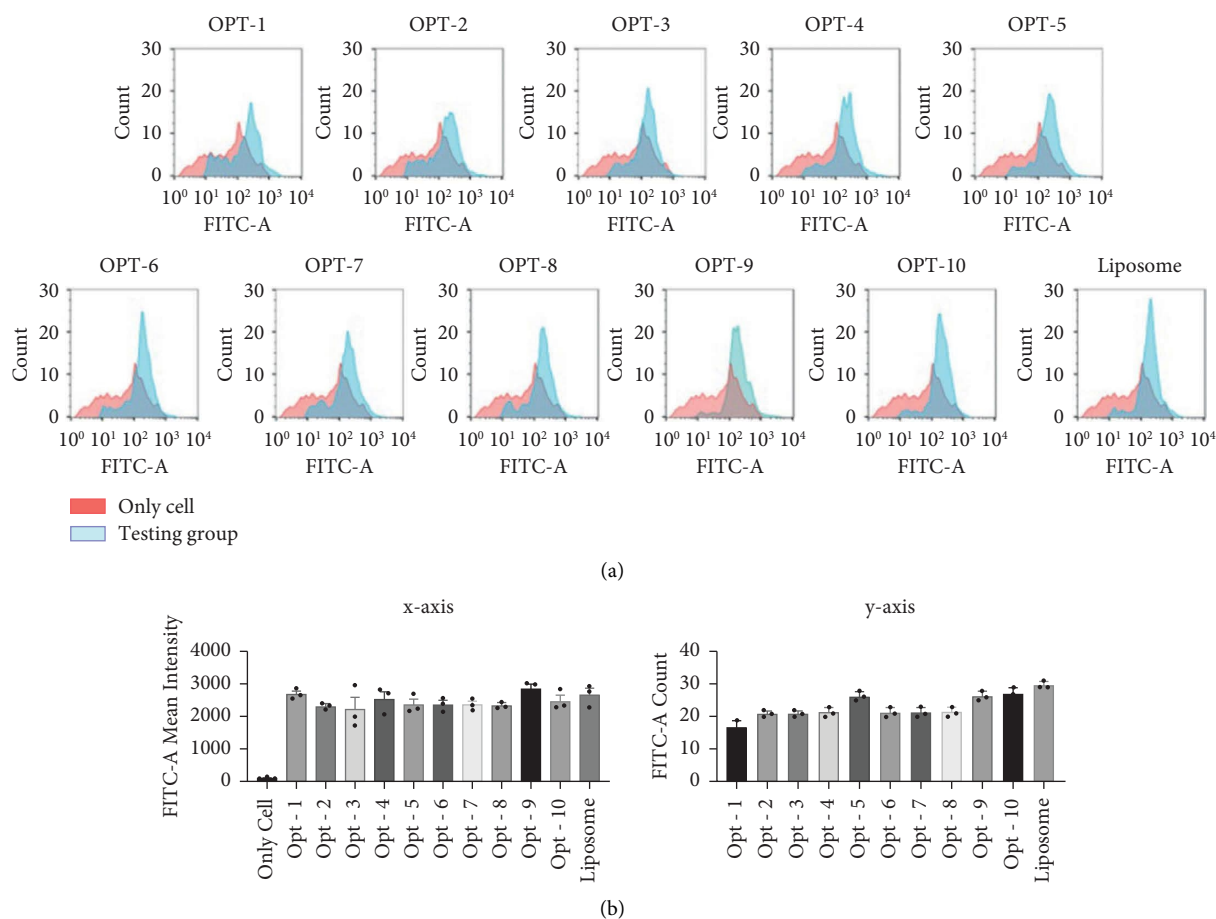
Figure 9: Simultaneous cellular uptake analysis performed for niosomal (Opt-1 to Opt-10) and liposomal (L-α-lecithin) formulations. Testing groups and a control group were represented as light blue and light red, respectively. (a) x-axis and y-axis shifts of test samples and their histogram overlay with only cell population. (b) Normalized FITC-A signal evaluation based on x-axis and y-axis shift. FITC, Fluorescein isothiocyanate.

Based on all these different analyses for stability, reproducibility, cytotoxicity, and cellular uptake analyses, we found that Opt-6, Opt-8, Opt-9, and Opt-10 were selected as the best formulations among all 10 different formulations (Supporting Figure 9). The cellular uptake results showed that even though liposomal and niosomal formulations had similar cellular viability profiles. The study also found that these four niosomal formulations were in the appropriate range in physicochemical characterization, stability, and reproducibility studies for further cellular applications.

The obtained results from flow cytometry and internalization assays suggest four niosomal formulations indicate similar performance with liposomes. To confirm the obtained results with visual data, confocal scanning fluorescence microscopy (CSFM) is used. FITC-tagged Opt-6, Opt-8, Opt-9, and Opt-10 are observed and compared with liposomes simultaneously. Supporting Figure 10 demonstrates recorded data for FITC-tagged nanoparticles and proposed enhanced internalization, especially as observed in Opt-10.

3.7. PTX Loading to Niosome.
Following the identification of optimal niosome formulation, Opt-10, we proceeded to load it with the chemotherapeutic agent, PTX, to evaluate its DLC and drug delivery efficiency. Based on previous studies, PTX-loaded niosomes are prepared at concentration ranging from 0.5 to 1 mg/mL [55, 56]. However, other studies have reported initial encapsulation of PTX-loaded niosomes at lower concentrations, such as 10 μg/mL [57]. In this study, we tested the EE% of Opt-10 using three PTX concentrations: 0.0125, 0.1, and 0.5 mg/mL. To calculate the EE%, a standard curve of PTX was generated with six different concentrations (Supporting Figure 12a). The resulting graph equation was applied to determine the amounts of encapsulated and free PTX. Although Opt-10 niosomes maintained their size within the desired range, the EE% decreased significantly as the PTX concentration increased from 0.0125 to 0.5 mg/mL (see Supporting Figure 12b). The physicochemical properties of PTX-loaded niosomes were analyzed using DLS, and the size distribution is depicted in Figure 10(a) and Supporting Figure 13a–13d. Table 4
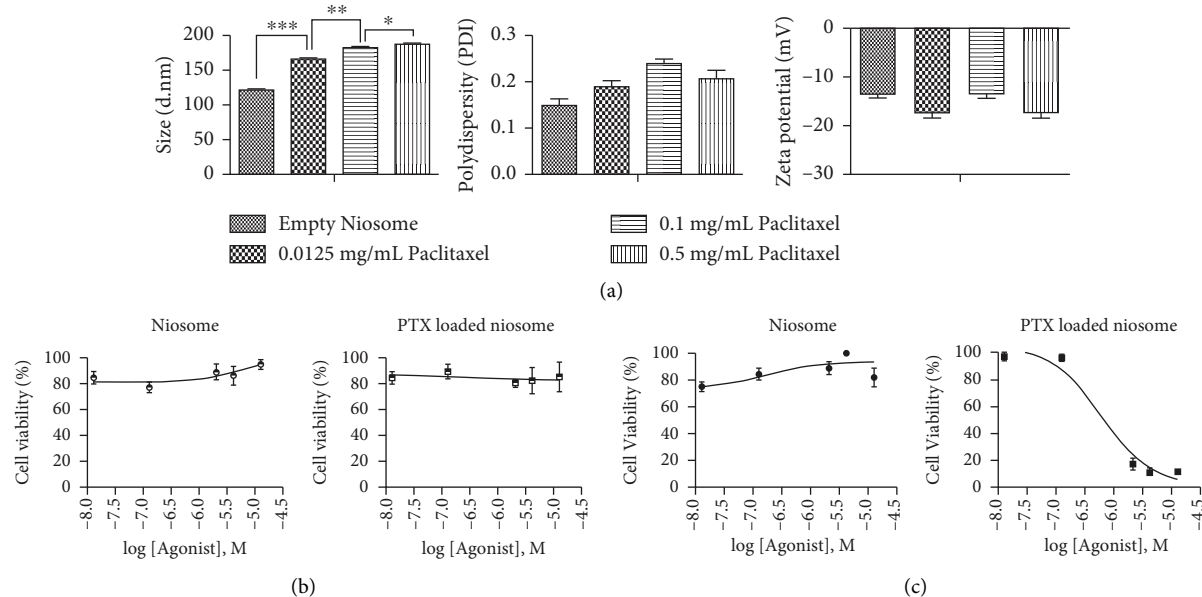
FIGURE 10: (a) DLS and zeta potential measurements of empty and PTX-loaded niosome (Opt-10). Error bars indicate standard deviation, and statistical test was performed by ANOVA with Tukey's multiple comparison; $^{*} p < 0.05$, $^{**} p < 0.001$, $^{***} p < 0.0001$. (b) Cell viability of empty niosome and PTX-loaded niosome (Opt-10) on HDF. (c) Cell viability of empty niosome and PTX-loaded niosome (Opt-10) on U87. ANOVA, Analysis of variance; DLS, dynamic light scattering; HDF, human-derived fibroblast; PTX, Paclitaxel.

TABLE 4: Drug encapsulation values of PTX-loaded niosomes.

#	Concentration (mg/mL)	EE (%)	DLC (%)	DLE (%)
1	0.0125	90.3 ± 2.6	9.2 ± 2.5	89.4 ± 3.7
2	0.1	14.7 ± 3.5	0.55 ± 0.06	13.2 ± 1.5
3	0.5	9.6 ± 2.1	0.11 ± 0.02	9.5 ± 0.3

Abbreviations: DLC, drug loading capacity; DLE, drug loading efficiency; EE, encapsulation efficiency.

presents the EE%, DLC%, and DLE% of PTX-loaded niosomes, calculated using the equations provided in the Methods section (equations (1)–(4)).

The results indicate that Opt-10 niosomes cannot be loaded with more than 0.5 mg/mL PTX without exceeding the target size range of 100–200 nm (Figure 10). The lowest concentration (0.0125 mg/mL) was chosen for subsequent experiment, as it achieved the highest EE% while maintaining the target size range (121 ± 12 nm) under optimized condition. Furthermore, we compared the cytotoxicity of unloaded niosomes and PTX-loaded niosomes on HDFs (Figure 10(b)) and U87 (Figure 10(c)). The results showed that unloaded niosomes exhibited no toxicity toward either cell line, while PTX-loaded niosomes were selectively cytotoxic to U87 cells, without affecting the healthy fibroblasts.

4. Conclusion

This study rigorously optimized niosomal nanoparticle formulations, conducting in-depth analyses of their physicochemical properties and cellular interactions, notably addressing a crucial research void through a comprehensive comparative examination alongside liposomes. Exploring diverse process parameters, it delineated pivotal size, polydispersity, and zeta potential ranges crucial for optimal niosome design, leveraging MODDE software to derive 10 refined formulations.

Significant findings highlighted the pronounced influence of surfactant types and the synergistic impact of concentration and sonication time on formulation outcomes. Importantly, this research identified indispensable size (100–200 nm), polydispersity (0.2–0.5), and zeta potential (−10 to 10 mV) thresholds essential for superior niosomal performance, bridging an important gap in simultaneous liposome–niosome comparisons. Extended stability assessments spanning 92 days demonstrated promising shelf-life profiles, showcasing formulations adhering consistently within specified critical ranges. Cellular studies revealed minimal toxicity and efficient uptake in select optimized niosomal formulations (Opt-6, Opt-8, Opt-9, and Opt-10), comparable to liposomes.

These refined niosomal formulations, boasting stability, reproducibility, low toxicity, and efficient cellular uptake akin to liposomes, signify their potential as economical and versatile nanocarriers. This pioneering comparative investigation with liposomes fills a significant research void, potentially reshaping drug delivery strategies and substantially elevating treatment efficacy and safety.

Data Availability Statement

All data generated or analyzed during this study are included in this published article (and its Supporting information files) or are available from the corresponding author upon request.

Disclosure

A preprint of the work has previously been deposited online [58].

Conflicts of Interest

The authors declare no conflicts of interest.

Funding

Acknowledgment

Supporting Information

Additional supporting information can be found online in the Supporting Information section. *(Supporting Information)*
Supporting information is available online, which includes the following data and profiles for niosomal formulations: polydispersity and zeta potential profiles of niosomal formulations; size distributions of different niosomal concentrations; polydispersity and zeta potential profiles of interday experiments; cellular viability of U87 cells and NFS-60 cells; standard curves for FITC labeling of liposomes and niosomes; flow cytometry data for FITC-labeled niosomes; FTIR analysis of liposomal and niosomal formulations; schematic summary for niosomal formulation characterization; confocal images; flow cytometry data at different incubation times of niosomes. Tables list detailed data for the analysis of the effect of sonication time by increased concentration for five different formulations; correlation analysis of formulation parameters for niosomal production; EE and FITC concentration optimizations; statistical analysis results for concentration and sonication time parameters based on preset criteria of size, PDI, and zeta potential; one-way ANOVA test results for the effect of the concentration parameter on PDI and zeta potential for each formulation; stability profiles of optimized formulations in terms of PDI for 21, 27, 35, and 92 days; stability profiles of optimized formulations in terms of zeta potential for 21, 27, 35, and 92 days; reproducibility profiles of optimized formulations in size (nm), PDI, and zeta potential (mV); and DLS data for liposomes.

References

[1] H. Ahmad, A. Arya, S. Agrawal, and A. K. Dwivedi, "Novel Lipid Nanostructures for Delivery of Natural Agents With Antioxidant, Antiinflammatory and Antistroke Potential: Perspectives and Outcomes," *Nanostructures for Oral Medicine* (Elsevier Inc, 2017), 577–605.

[2] G. Aggarwal, S. Bansal, P. Chandel, and S. L. Harikumar, "Design and Development of Cefdinir Niosomes for Oral Delivery," *Journal of Pharmacy and BioAllied Sciences* 5, no. 4 (2013): 318–325, https://doi.org/10.4103/0975-7406.120080.

[3] P. Aparajay and A. Dev, "Functionalized Niosomes as a Smart Delivery Device in Cancer and Fungal Infection," *European Journal of Pharmaceutical Sciences* 168 (2022): 106052, https://doi.org/10.1016/j.ejps.2021.106052.

[4] M. I. El Dosoky and A. M. Ahmad, "Glutathione—Loaded Non—Ionic Surfactant Niosomes: A New Approach to Improve Oral Bioavailability and Hepatoprotective Efficacy of Glutathione" (2022), 117–137.

[5] B. A. Ibrahim, "Chapter 7—Liposomes-And Niosomes-Based Drug Delivery Systems for Tuberculosis Treatment," in *Kesharwani PBT-NBA for TT Editor* (Cambridge, MA: Academic Press, 2020).

[6] M. J. Mitchell, M. M. Billingsley, R. M. Haley, M. E. Wechsler, N. A. Peppas, and R. Langer, "Engineering Precision Nanoparticles for Drug Delivery," *Nature Reviews Drug Discovery* 20, no. 2 (2021): 101–124, https://doi.org/10.1038/s41573-020-0090-8.

[7] Y. Fan, M. Marioli, and K. Zhang, "Analytical Characterization of Liposomes and Other Lipid Nanoparticles for Drug Delivery," *Journal of Pharmaceutical and Biomedical Analysis* 192 (2021): 113642, https://doi.org/10.1016/j.jpba.2020.113642.

[8] D. B. G and V. L. P, "Recent Advances of Non-Ionic Surfactant-Based Nano-Vesicles (Niosomes and Proniosomes): A Brief Review of These in Enhancing Transdermal Delivery of Drug," *Future Journal of Pharmaceutical Sciences* 6 (2020): 100–118, https://doi.org/10.1186/s43094-020-00117-y.

[9] P. van Hoogevest, X. Liu, and A. Fahr, "Drug Delivery Strategies for Poorly Water-Soluble Drugs: The Industrial Perspective," *Expert Opinion on Drug Delivery* 8, no. 11 (2011): 1481–1500, https://doi.org/10.1517/17425247.2011.614228.

[10] N. O. Dhoot and M. A. Wheatley, "Microencapsulated Liposomes in Controlled Drug Delivery: Strategies to Modulate Drug Release and Eliminate the Burst Effect," *Journal of Pharmaceutical Sciences* 92, no. 3 (2003): 679–689, https://www.sciencedirect.com/science/article/pii/S0022354916312011, https://doi.org/10.1002/jps.19104.

[11] A. Catarina, J. Nuno, and S. Simoes, "Combination Chemotherapy in Cancer: Principles, Evaluation and Drug Delivery Strategies," *Current Cancer Treatment—Novel Beyond Conventional Approaches* (London, UK: Intechopen, 2011).

[12] J. Varshosaz and S. Taymouri, "Effect of Different Types of Surfactants on the Physical Properties and Stability of Carvedilol Nano-Niosomes," *Advanced Biomedical Research* 5, no. 1 (2016): 48, https://doi.org/10.4103/2277-9175.178781.

[13] A. De, N. Venkatesh, M. Senthil, B. K. R. Sanapalli, R. Shanmugham, and V. V. S. R. Karri, "Smart Niosomes of Temozolomide for Enhancement of Brain Targeting," *Nanobiomedicine* 5 (2018): 1849543518805355, https://doi.org/10.1177/1849543518805355.

[14] M. Rezaeizadeh, A. Eskanlou, H. Soltani, A. Pardakhty, M. H. Moshafi, and F. Hosseini-Nejad, "Preparation of Stable Clindamycin Phosphate Niosomes by Combination of Sorbitan Esters and Their Ethoxylaed Derivatives," *Journal of Pharmaceutical Innovation* 17, no. 4 (2021): 1189–1198, https://doi.org/10.1007/s12247-021-09594-x.

[15] A. Miatmoko, S. Safitri, F. Aquila, et al., "Characterization and Distribution of Niosomes Containing Ursolic Acid Coated With Chitosan Layer," *Research in Pharmaceutical Sciences* 16, no. 6 (2021): 660–673, https://doi.org/10.4103/1735-5362.327512.

[16] L. K. Yeo, C. S. Chaw, and A. A. Elkordy, "The Effects of Hydration Parameters and Co-Surfactants on Methylene Blue-Loaded Niosomes Prepared by the Thin Film Hydration Method," *Pharmaceuticals* 12, no. 2 (2019): 46, https://doi.org/10.3390/ph12020046.

[17] W. Zeng, Q. Li, T. Wan, et al., "Hyaluronic Acid-Coated Niosomes Facilitate Tacrolimus Ocular Delivery: Mucoadhesion, Precorneal Retention, Aqueous Humor Pharmacokinetics, and Transcorneal Permeability," *Colloids and Surfaces B: Biointerfaces* 141 (2016): 28–35, https://doi.org/10.1016/j.colsurfb.2016.01.014.

[18] A. Manosroi, P. Khanrin, W. Lohcharoenkal, et al., "Transdermal Absorption Enhancement Through Rat Skin of Gallidermin Loaded in Niosomes," *International Journal of Pharmaceutics* 392, no. 1-2 (2010): 304–310, https://www.sciencedirect.com/science/article/pii/S0378517310002711, https://doi.org/10.1016/j.ijpharm.2010.03.064.

[19] C. Marianecci, D. Paolino, C. Celia, M. Fresta, M. Carafa, and F. Alhaique, "Non-Ionic Surfactant Vesicles in Pulmonary Glucocorticoid Delivery: Characterization and Interaction With Human Lung Fibroblasts," *Journal of Controlled Release* 147, no. 1 (2010): 127–135, https://www.sciencedirect.com/science/article/pii/S0168365910004700, https://doi.org/10.1016/j.jconrel.2010.06.022.

[20] L. Tavano, R. Muzzalupo, N. Picci, and B. de Cindio, "Co-Encapsulation of Antioxidants Into Niosomal Carriers: Gastrointestinal Release Studies for Nutraceutical Applications," *Colloids and Surfaces B: Biointerfaces* 114 (2014): 82–88, https://doi.org/10.1016/j.colsurfb.2013.09.058.

[21] M. Esmaeili Rad, A. C. Egil, G. Ozaydin Ince, M. Yuce, and A. Zarrabi, "Optimization of Curcumin Loaded Niosomes for Drug Delivery Applications," *Colloids and Surfaces A: Physicochemical and Engineering Aspects* 654 (2022): 129921, https://www.sciencedirect.com/science/article/pii/S0927775722016764, https://doi.org/10.1016/j.colsurfa.2022.129921.

[22] P. Trucillo, "Industrial Approach," *Processes* 9 (2021): 1–18.

[23] E. A. Simone, T. D. Dziubla, and V. R. Muzykantov, "Polymeric Carriers: Role of Geometry in Drug Delivery," *Expert Opinion on Drug Delivery* 5, no. 12 (2008): 1283–1300, https://doi.org/10.1517/17425240802567846.

[24] I. Khan, K. Saeed, and I. Khan, "Nanoparticles: Properties, Applications and Toxicities," *Arabian Journal of Chemistry* 12, no. 7 (2019): 908–931, https://doi.org/10.1016/j.arabjc.2017.05.011.

[25] W. H. De Jong and P. J. A. Borm, "Drug Delivery and Nanoparticles: Applications and Hazards," *International Journal of Nanomedicine* 3, no. 2 (2008): 133–149, https://doi.org/10.2147/ijn.s596.

[26] D. T. Savage, J. Z. Hilt, and T. D. Dziubla, "In Vitro Methods for Assessing Nanoparticle Toxicity," *Methods in Molecular Biology* 1894 (2019): 1–29, https://doi.org/10.1007/978-1-4939-8916-4_1.

[27] S. Behzadi, V. Serpooshan, W. Tao, et al., "Cellular Uptake of Nanoparticles: Journey Inside the Cell," *Chemical Society Reviews* 46, no. 14 (2017): 4218–4244, https://doi.org/10.1039/c6cs00636a.

[28] Z.-J. Zhu, P. S. Ghosh, O. R. Miranda, R. W. Vachet, and V. M. Rotello, "Multiplexed Screening of Cellular Uptake of Gold Nanoparticles Using Laser Desorption/Ionization Mass Spectrometry," *Journal of the American Chemical Society* 130 (2008): 14139–14143, https://doi.org/10.1021/ja805392f.

[29] G. Singh, A. Faruk, and P. M. S. Bedi, "Spectral Analysis of Drug Loaded Nanoparticles for Drug-Polymer Interactions," *Journal of Drug Delivery and Therapeutics* 8, no. 6 (2018): 111–118, https://doi.org/10.22270/jddt.v8i6.2030.

[30] N. Kamaraj, P. Y. Rajaguru, P. K. Issac, and S. Sundaresan, "Fabrication, Characterization, In Vitro Drug Release and Glucose Uptake Activity of 14-Deoxy, 11,12-Didehydroandrographolide Loaded Polycaprolactone Nanoparticles," *Asian Journal of Pharmaceutical Sciences* 12, no. 4 (2017): 353–362, https://doi.org/10.1016/j.ajps.2017.02.003.

[31] M. Yaghoobian, A. Haeri, N. Bolourchian, S. Shahhosseni, and S. Dadashzadeh, "The Impact of Surfactant Composition and Surface Charge of Niosomes on the Oral Absorption of Repaglinide as a BCS II Model Drug," *International Journal of Nanomedicine* 15 (2020): 8767–8781, https://pubmed.ncbi.nlm.nih.gov/33204087, https://doi.org/10.2147/ijn.s261932.

[32] P. Shah, B. Goodyear, A. Haq, V. Puri, and B. Michniak-Kohn, "Evaluations of Quality by Design (QbD) Elements Impact for Developing Niosomes as a Promising Topical Drug Delivery Platform," *Pharmaceutics* 12, no. 3 (2020): 246, https://doi.org/10.3390/pharmaceutics12030246.

[33] Y. Thabet, M. Elsabahy, and N. G. Eissa, "Methods for Preparation of Niosomes: A Focus on Thin-Film Hydration Method," *Methods* 199 (2022): 9–15, https://www.sciencedirect.com/science/article/pii/S1046202321001304, https://doi.org/10.1016/j.ymeth.2021.05.004.

[34] A. Mishra and P. Gupta, "Gastro Retentive Drug Delivery System: A Review," *International Journal of Drug Development and Research* 4 (2012): 28–39.

[35] B. A. Ibrahim, "Chapter 7—Liposomes-and Niosomes-Based Drug Delivery Systems for Tuberculosis Treatment," in *Kesharwani PBT-NBA for TT Editor* (Cambridge: Academic Press, 2020), https://www.sciencedirect.com/science/article/pii/B9780128198117000072.

[36] X. Ge, M. Wei, S. He, and W.-E. Yuan, "Advances of Non-Ionic Surfactant Vesicles (Niosomes) and Their Application in Drug Delivery," *Pharmaceutics* 11, no. 2 (2019): 55, https://pubmed.ncbi.nlm.nih.gov/30700021, https://doi.org/10.3390/pharmaceutics11020055.

[37] R. Ghafelehbashi, I. Akbarzadeh, M. Tavakkoli Yaraki, A. Lajevardi, M. Fatemizadeh, and L. Heidarpoor Saremi, "Preparation, Physicochemical Properties, In Vitro Evaluation and Release Behavior of Cephalexin-Loaded Niosomes,"

International Journal of Pharmaceutics 569 (2019): 118580, https://doi.org/10.1016/j.ijpharm.2019.118580.

[38] M. Silindir-Gunay, M. Karpuz, N. Ozturk, A. Yekta Ozer, S. Erdogan, and M. Tuncel, "Radiolabeled, Folate-Conjugated Liposomes as Tumor Imaging Agents: Formulation and In Vitro Evaluation," *Journal of Drug Delivery Science and Technology* 50 (2019): 321–328, https://doi.org/10.1016/j.jddst.2019.02.003.

[39] H. M. Hnin, E. Stefánsson, T. Loftsson, R. Asasutjarit, D. Charnvanich, and P. Jansook, "Physicochemical and Stability Evaluation of Topical Niosomal Encapsulating Fosinopril/γ-Cyclodextrin Complex for Ocular Delivery," *Pharmaceutics* 14, no. 6 (2022): 1147, https://doi.org/10.3390/pharmaceutics14061147.

[40] P. Álamo, V. Pallarès, M. V. Céspedes, et al., "Fluorescent Dye Labeling Changes the Biodistribution of Tumor-Targeted Nanoparticles," *Pharmaceutics* 12, no. 11 (2020): 1004, https://doi.org/10.3390/pharmaceutics12111004.

[41] T. Thomsen, A. B. Ayoub, D. Psaltis, and H.-A. Klok, "Fluorescence-Based and Fluorescent Label-free Characterization of Polymer Nanoparticle Decorated T Cells," *Biomacromolecules* 22, no. 1 (2021): 190–200, https://doi.org/10.1021/acs.biomac.0c00969.

[42] K. Anzai, M. Yoshida, and Y. Kirino, "Change in Intravesicular Volume of Liposomes by Freeze-Thaw Treatment as Studied by the ESR Stopped-Flow Technique," *Biochimica et Biophysica Acta (BBA)—Biomembranes* 1021, no. 1 (1990): 21–26, https://www.sciencedirect.com/science/article/pii/0005273690903782, https://doi.org/10.1016/0005-2736(90)90378-2.

[43] R. I. MacDonald and R. C. MacDonald, "Lipid Mixing During Freeze-Thawing of Liposomal Membranes as Monitored by Fluorescence Energy Transfer," *Biochimica et Biophysica Acta (BBA)—Biomembranes* 735, no. 2 (1983): 243–251, https://doi.org/10.1016/0005-2736(83)90299-7.

[44] M. Khan, M. M. Hasan, A. Barnett, et al., "Co-Axial Electrospraying of Injectable Multi-Cancer Drugs Nanocapsules With Polymer Shells for Targeting Aggressive Breast Cancers," *Cancer Nanotechnology* 13, no. 1 (2022): 6, https://doi.org/10.1186/s12645-022-00114-1.

[45] S. Joshi, R. White, R. Sahu, V. A. Dennis, and S. R. Singh, "Comprehensive Screening of Drug Encapsulation and Co-Encapsulation Into Niosomes Produced Using a Microfluidic Device," *Processes* 8, no. 5 (2020): 535, https://doi.org/10.3390/pr8050535.

[46] H. M. Owais, M. M. Baddour, H. A. E.-R. El-Metwally, H. S. Barakat, N. S. Ammar, and M. A. Meheissen, "Assessment of the In Vitro Activity of Azithromycin Niosomes Alone and in Combination With Levofloxacin on Extensively Drug-Resistant *Klebsiella pneumoniae* Clinical Isolates," *Brazilian Journal of Microbiology* 52, no. 2 (2021): 597–606, https://doi.org/10.1007/s42770-021-00433-2.

[47] D. Ag Seleci, M. Seleci, J. G. Walter, F. Stahl, and T. Scheper, "Niosomes as Nanoparticular Drug Carriers: Fundamentals and Recent Applications," *Journal of Nanomaterials* 2016 (2016): 1–13, https://doi.org/10.1155/2016/7372306.

[48] C. M. Beddoes, C. P. Case, and W. H. Briscoe, "Understanding Nanoparticle Cellular Entry: A Physicochemical Perspective," *Advances in Colloid and Interface Science* 218 (2015): 48–68, https://doi.org/10.1016/j.cis.2015.01.007.

[49] E. Blanco, H. Shen, and M. Ferrari, "Principles of Nanoparticle Design for Overcoming Biological Barriers to Drug Delivery," *Nature Biotechnology* 33, no. 9 (2015): 941–951, https://pubmed.ncbi.nlm.nih.gov/26348965, https://doi.org/10.1038/nbt.3330.

[50] J. L. White, "Interpretation of Infrared Spectra of Soil Minerals," *Soil Science* 112, no. 1 (1971): 22–31, https://doi.org/10.1097/00010694-197107000-00005.

[51] V. J. Mokale, H. I. Patil, A. P. Patil, P. R. Shirude, and J. B. Naik, "Formulation and Optimisation of Famotidine Proniosomes: An In Vitro and Ex Vivo Study," *Journal of Experimental Nanoscience* 11, no. 2 (2016): 97–110, https://doi.org/10.1080/17458080.2015.1030711.

[52] M. Takikawa, M. Fujisawa, K. Yoshino, and S. Takeoka, "Intracellular Distribution of Lipids and Encapsulated Model Drugs from Cationic Liposomes With Different Uptake Pathways," *International Journal of Nanomedicine* 15 (2020): 8401–8409, https://pubmed.ncbi.nlm.nih.gov/33149583, https://doi.org/10.2147/ijn.s267638.

[53] F. Li, M. Yang, L. Wang, et al., "Autofluorescence Contributes to False-Positive Intracellular Foxp3 Staining in Macrophages: A Lesson Learned From Flow Cytometry," *Journal of Immunological Methods* 386, no. 1-2 (2012): 101–107, https://doi.org/10.1016/j.jim.2012.08.014.

[54] V. L. Mosiman, B. K. Patterson, L. Canterero, and C. L. Goolsby, "Reducing Cellular Autofluorescence in Flow Cytometry: An In Situ Method," *Cytometry* 30, no. 3 (1997): 151–156, https://doi.org/10.1002/(sici)1097-0320(19970615)30:3%253A151::aid-cyto6%253E3.3.co;2-g.

[55] F. Raza, H. Zafar, M. W. Khan, et al., "Recent Advances in the Targeted Delivery of Paclitaxel Nanomedicine for Cancer Therapy," *Materials Advances* 3, no. 5 (2022): 2268–2290, https://doi.org/10.1039/d1ma00961c.

[56] P. S. Jadon, S. Nayak, and S. K. Singh, "Formulation and Optimization of Niosomes for Targeted Delivery of Paclitaxel," *Asian Journal of Pharmaceutics* 12, no. 1 (2018): 20–31.

[57] S. Kamboj, H. Gupta, and S. Jain, "Niosomes: An Excellent Tool for Drug Delivery," *International Journal of Research in Pharmacy and Chemistry* 4, no. 2 (2014): 339–349.

[58] N. Cakir, N. Ozturk, A. Kara, A. Zarrabi, and N. Mustafaoglu, "Optimizing Niosome Formulations for Enhanced Cellular Applications: A Comparative Case Study With L-α-Lecithin Liposomes," *Preprint* https://www.biorxiv.org/content/10.1101/2023.11.14.567080v1.